# NUMERICAL INVESTEGATION OF BOUNDARY LAYER TRANSITION OVER FLAT-PLATE

KUNLUN LIU, KHOON SENG YEO
AND
CHANG SHU, ZHENGYI WANG

*Department of Mechanical Engineering,*
*National University of Singapore*
*10 Kent Ridge Crescent, Singapore, 119260*

**Abstract**

This paper presents two numerical cases of disturbed Navier-Stokes equations. In case 1, four order accuracy finite difference is used to investigate the evolution of negative frequency disturbance in Blasius boundary layer, results show us that negative frequency can reduce the streamwise wavelength of T-S wave, and accelerate the transition process. The effect of negative frequency lets to the breakdown of fluid structure becomes more significant. And, in the case two, two order accuracy finite volume method is used, Reynolds number is 900, and dimensionless frequency F is 86 in this case. Results present that the evolution process is more gradual in the positive frequency compare with the negative frequency in case 1. And the pressure contours clearly present a nonlinear interaction and break down process of two $\lambda$ vortexes.

## 1. Introduction.

The laminar-turbulent transition is long interested by researchers of fluid dynamics. Stability theory has been developed as a theoretical understand of transition phenomena, its early period is the stage of linear theory, L. Prandtl[1], W. Tollmien and Grohne, D[2], W. Heisenberg[3] and C. C. Lin[4] greatly contributed to it. The character of this period is the development of theoretical work is faster than that of experiment and computation. Up to 1947, by the using of ribbon technique, G. B. Schubauer and H. K. Skramstad[5] successfully got powerful experiment supports of the linear stability theory.

Since the breakthrough in experiment and computation, experiment and computation quickly developed, and quickly beyond the development of theoretical work, because the difficulty in non-linear analysis obstructs its advance. The most important achievements in the stability theory during this period is the discovery of C-type[6], H-type[7,8], K-type[9] and N-type[10, 11] breakdown. C-type breakdown can be explained by triad resonance theory, and H-type

breakdown can be explained by the secondary instability theory. The experiments of Saric and Tomas[12] show that for the different amplitude of T-S wave, fluid will transition on the different breakdown route. When the amplitude of T-S wave range from 0.2% to 0.4%, the flows will present C-type instability, and the amplitude of T-S wave range from 0.4% to 0.6%, H-type instability will appear in flow. When the amplitude of T-S wave is over 0.6%, the k-type instability will appear. Since the secondary instability bases on the assumption that T-S wave is independent with the secondary disturbance, when the amplitude of T-S wave is high enough, this condition can be easily satisfied. This is the reason H-type breakdown happen on the higher amplitude T-S wave conditions compare with C-type breakdown. Since the clear, directly and universal theoretical analysis about Navier-Stokes equation has been unavailable up to now because of the nonlinear difficulty, numerical simulation become the necessary tool to the stability theory. H. Fasel[13, 14], B. J. Bayly & S. A. Orsag[15] and C. Liu & Z. Liu[16] got some excellent numerical simulated results of transition in the different cases.

The purpose of this paper is to present the nonlinear interaction of fluid structure, and effect of frequency to transition.

## 2. Governing equation and numerical method.

Fluid field is decomposed into two parts: mean flow and disturbance. The mean flow in our cases is Blasius boundary layer. The governing equations become:

$$\frac{\partial u_i}{\partial t}+J[(\frac{\partial u_i(U_1+U_1^0)+u_i^0U_1}{\partial \xi})+(\frac{\partial u_i(U_2+U_2^0)+u_i^0U_2}{\partial \eta})+(\frac{\partial u_i(U_3+U_3^0)+u_i^0U_3}{\partial \varsigma})]+$$

$$(\xi_i\frac{\partial}{\partial \xi}+\eta_i\frac{\partial}{\partial \eta}+\varsigma_i\frac{\partial}{\partial \varsigma})p-\frac{\Delta u_i}{\mathrm{Re}}=0 \qquad (1.1)$$

$$\frac{\partial u_1}{\partial \xi}+\frac{\partial u_2}{\partial \eta}+\frac{\partial u_3}{\partial \varsigma}=0 \qquad (1.2)$$

where $u_i$ are disturbed velocity components, $p$ is disturbed pressure, $J$ is transformation Jacobian, $u_i^0$ are mean flow velocity components. $U_i$ and $U_i^0$ are contravariant disturbance velocity components and contravariant mean flow velocity components, and hold:

$$U_1=\frac{1}{J}(u_1\xi_x+u_2\xi_y+u_3\xi_z),\quad U_2=\frac{1}{J}(u_1\eta_x+u_2\eta_y+u_3\eta_z),$$

$$U_3=\frac{1}{J}(u_1\varsigma_x+u_2\varsigma_y+u_3\varsigma_z)$$

$$U_1^0 = \frac{1}{J}(u_1^0\xi_x + u_2^0\xi_y + u_3^0\xi_z),\ U_2^0 = \frac{1}{J}(u_1^0\eta_x + u_2^0\eta_y + u_3^0\eta_z),$$

$$U_3^0 = \frac{1}{J}(u_1^0\varsigma_x + u_2^0\varsigma_y + u_3^0\varsigma_z)$$

Inflow displacement thickness is used as dimensionless constant. The following orthogonal grids are used for the numerical simulation:

$$x = \xi, \qquad y = \frac{y_{\max}\sigma\eta}{\eta_{\max}\sigma + y_{\max}(\eta_{\max} - \eta)}, \qquad z = \varsigma \tag{2}$$

in both case, $y_{\max} = 40$, and $\sigma = 6$. And the grids are homogeneous in the streamwise and spanwise. For preventing the pressure-velocity couple, staggered grid is used.

We simulate two different cases for the description the evolutions and interaction of T-S wave in flat-plate boundary layer transition. The first case focus on the effect of negative frequency disturbance to the transition, we wish numerical results could present the phenomena that the negative frequency disturbance will greatly accelerate the breakdown process. And for this purpose, finite difference method with second-order backward Euler differences in time direction and fourth-order central differences in space direction is used. The inflow is the superposition of solutions of O-S equation, and holds:

$$u_i = \phi(\eta)_i^{2d} e^{i(-\omega t)} + \phi(\eta)_i^{3d} e^{i(-\omega t + \beta\varsigma)} + \phi(\eta)_i^{3d} e^{i(-\omega t - \beta\varsigma)} + C.C. \tag{3.1}$$

$$p = \phi'(\eta)^{2d} e^{i(-\omega t)} + \phi'(\eta)^{3d} e^{i(-\omega t + \beta\varsigma)} + \phi'(\eta)^{3d} e^{i(-\omega t - \beta\varsigma)} + C.C. \tag{3.2}$$

The side condition is periodic, which hold:

$$\phi_{i,j,1} = \phi_{i,j,NK+1}, \qquad \phi_{i,j,NK+2} = \phi_{i,j,2} \tag{4}$$

So every periodic in spanwise direction will be investigated by $K+1$ point. And the length of spanwise is set as:

$$L_k = \frac{2\pi(NK+1)}{\beta K} \tag{5}$$

For avoiding the numerical divergence in the outflow region, the previous work[16] use buffer zone technique in the outflow region. But in case one, we replace the buffer zone technique with the first order upwind scheme, by the numerical dispassion of upwind scheme, the numerical divergence is successfully avoided. The using of upwind scheme bases on the following consider, when the transition happen, the large scale vortex structure will grow up, if the outflow boundary locate at the center of this large scale vortex, the outer flow boundary will hold the symmetric boundary condition, such as

$$\phi_{I-1/2} = \phi_{I+1/2}, \qquad \phi'_{I-1/2} = -\phi'_{I+1/2}$$

where $I$ is the grid of outer boundary. In this condition, we have the following relation:

$$\frac{\partial f}{\partial \xi}=\frac{f^*_{i+1/2}-f^*_{i-1/2}}{\Delta\xi}=\frac{(f_{i+1}-f_{i-1})-|A|_{i+1/2}\Delta U_{i+1/2}+|A|_{i-1/2}\Delta U_{i-1/2}}{\Delta\xi}=\frac{2|A|_{i-1/2}\Delta U_{i-1/2}}{\Delta\xi}$$

So

$$\frac{\partial U}{\partial t}+\frac{\partial f}{\partial \xi}+\frac{\partial p}{\partial \xi}-\frac{\partial^2 f_v}{\mathrm{Re}\,\partial\xi\partial\xi}=\frac{U^{n+1}-U^n}{\Delta t}+\frac{2|A|_{i-1/2}\Delta U_{i-1/2}}{\Delta\xi}+\frac{\partial p}{\partial \xi}-\frac{\partial^2 f_v}{\mathrm{Re}\,\partial\xi\partial\xi} \quad (6)$$

This is obvious that (6) has upwind character; this kind of boundary condition can help to prevent the numerical divergence.

In the second case, the disturbance;

$$u_1=\varepsilon_1^{2d}e^{i(-\omega t)}+\varepsilon_1^{3d}e^{i(-\omega t+\beta\varsigma)}+\varepsilon_1^{3d}e^{i(-\omega t-\beta\varsigma)}+C.C. \quad (7.1)$$

$$u_2=u_3=p=0 \quad (7.2)$$

is introduced on the wall, and the position is $(i',1,k)$. We use this kind of disturbance to simulate the behavior of disturbance, which is excited by a ribbon on the wall. The two order spatial accuracy and two order temporal accuracy SIMPLE method is used.

## 2. Results and Conclusions.

In the case 1, the Reynolds number 900 and 800 are simulated, and $\beta$ is 0.1. In this case, we set $\phi_i^{2d}=2\phi_i^{3d}$, the wavelength of (3.1) and (3.2) on the spanwise direction will reduce to its half, $\frac{\beta}{2}$. Therefore, a subharmonic, which holds a half frequency of T-S wave, generates. The numerical grid of case 1 is $160\times36\times32$. Since the early part of transition is a spatial instability dominant, wave number is real, so we assume that the dimensionless frequency is –86, according to analysis of A. H. Nayfeh and A. Padhyen[17], the group speed hold:

$$\frac{\partial\omega}{\partial a}=C_g e^{i\chi}=\frac{d\xi}{dt}\Big|_{(T-S\ wave)} \quad (8)$$

where $\chi$ is the phase angel of group speed. Therefore, for the T-S wave, we can get the following formula:

$$\phi(\eta)e^{i(-\omega t+\alpha\xi)}=\phi(\eta)\exp[i(a\xi-\omega\int_{t_0}^{t}dt)]=\phi(\eta)\exp[i(a\xi-\omega\int_{t_0}^{t}\frac{d\xi}{C_g e^{i\chi}})] \quad (9)$$

Our numerical results in case 1 (fig.1~fig.3) proves that in the first 4 or 5 T-S wave, the group speed of T-S wave is homogenous. Therefore, from (9), it obtains that:

$$\phi(\eta)e^{i(-\omega t+\alpha\xi)} = \phi(\eta)\exp[i(a-\omega\left\langle\frac{1}{C_g e^{i\chi}}\right\rangle)\xi] \tag{10}$$

where $\langle\cdot\rangle$ stands for the average in a streamwise wavelength. From (10), we get a formula of streamwise wavelength $l_{wave}$:

$$l_{wave} = 2\pi/(a_{re}-\omega\left\langle\frac{1}{C_g e^{i\chi}}\right\rangle) \tag{11}$$

where $a_{re}$ is the real part of $a$. Although the wave number of case 1 is negative, the propagation direction of T-S wave and the direction of group speed are still positive, which are along the streamwise. Therefore, the wavelength $l_{wave}$ of case 1 is shorter than the condition of corresponding positive frequency, such as case 2.

Figure 1, 2 and 3 are consequences of case 1, Figure 2 clearly present that, in the second periodic of T-S wave, it breaks into two parts in the spanwise, this is a typical harmonica behavior. As the evolution of T-S wave, structures continuously break down; fluid contour becomes more and more irregular and complex. Turbulence happens. The strength of the amplitude of disturbance in figure 3 is higher than that of figure 1 and figure 2, and $\max(\phi_i^{2d}) = 0.04$ in figure 3, and $\max(\phi_i^{2d}) = 0.02$ in figure 1 and figure 2, where $\phi_i^{2d}$ is the profile of coming flow.

Figure 4 to 11 are numerical result of case 2. In this case, Reynolds number is 900, $\beta$ is 0.1, and the dimensionless frequency F is 86. But, in case 2, $\phi_i^{2d} = 3\phi_i^{3d}$. The numerical grid is $140\times32\times32$. Numerical ribbon sets on the grids $(30,1,k)$. The maximum receptive velocity on the $(30,2,k)$ is 0.005. Results clearly show us an entire interaction process of two $\lambda$ vortexes. At first, each $\lambda$ vortex will be stretched by the other, their head will move closely in their propagation direction. In the region $\mathrm{Re} = 1200$, two $\lambda$ vortexes merge together. And, quickly, breakdown happens.

## REFRENCE

[1]Prandtl, L. 1931, Über die Entstehung der Turbulenz. *ZAMM*, **11**, 407.

[2]Tollmien, W. and Grohne, D. 1961, *The nature of transition, In: Boundary Layer and Flow Control.* **Vol.2,** Pergamon Press, London.

[3]Heisenberg, W. 1924, Über Stabilität und Turbulenz von Flüssigkeitsströmen. *Ann. D. Phys.* **74**, 577.

[4]Lin, C. C. 1955, The theory of hydrodynamic stability, Cambridge Univ. Press.

[5]Schubauer, G. B., Skramstad, H. H., 1947, Laminar boundary layer oscilliations and stability of laminar flow, NACA Tech. Report No. 909.

[6]Craik, A. D. D. 1971, Non-Linear resonant instability in boundary layers. *J. Fluid Mech.* **50**, 393.

[7]Herbert, Th. 1983, Secondary instability of plane channel flow to subharmonic three-dimensional disturbances. *Phys. Fluids.* **26(4)**, 871.

[8]Herbert, Th. 1988, Secondary instability of boundary Layers. *Ann. Rev. Fluid. Mech.* **20**, 487.

[9]Klebanoff, P. S., Tidstrom, K. D. & Sargent, L. M. 1962, The three-dimensional nature of boundary-layer instability. *J. Fluid Mech.* **12**, 1.

[10]Kachanov, Y. S. 1987, On the resonant nature of the breakdown of a laminar boundary layer. *J. Fluid Mech.* **184**, 43.

[11]Kachanov, Y. S. 1994, Physical mechanisms of laminal-boundary-layer transition. *Ann. Rev. Fluid. Mech.* **26**, 411.

[12]Saric, W. S. and Thomas, A. S. W. 1984, Experiments on the subharmonic route to turbulence in boundary layers, *Turbulence and Chaotic Phenomena in Fluids.* (ed. T. Tatsumi), pp. 117~122. North-Holland.

[13]Fasel, H. 1976, Investigation of the stability of boundary layers by a finite differencemodel of the Navier-Stokes equations. *J. Fluid Mech.* **78**, 355.

[14]Fasel, H. and Konzelmann, U. 1990, Non-parallel stability of a flat-plate boundary layer using the complete Navier-Stokes equations. *J. Fluid Mech.* **221**, 311.

[15]Baylay, B. J. and Orszag, S. A. 1988, Instability mechanisms in shear-flow transition. *Ann. Rev. Fluid. Mech.* **26**, 411.

[16]Liu, C. & Liu, Z., 1995, Multigrid mapping and box relaxation for simulation of the whole process of flow transition in 3d boundary layer, *J. Comp. Phy.* **119**, 325.

[17]Nayfeh A. H. and Padhyen A. 1979, *AIAA Jour.* **17.** 1084~1090.

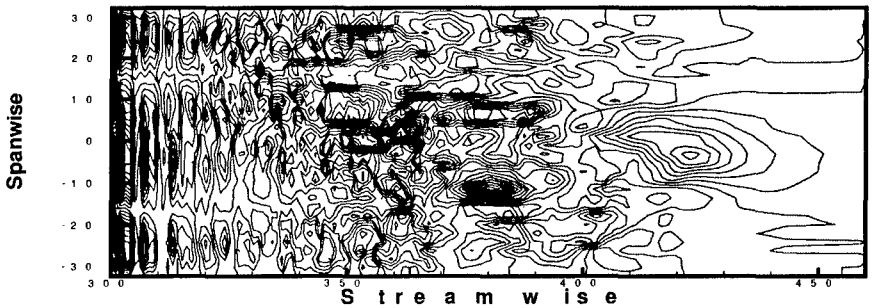


Figure 1, Spanwise velocity contour, Re = 900, F = 86. y = 2.0

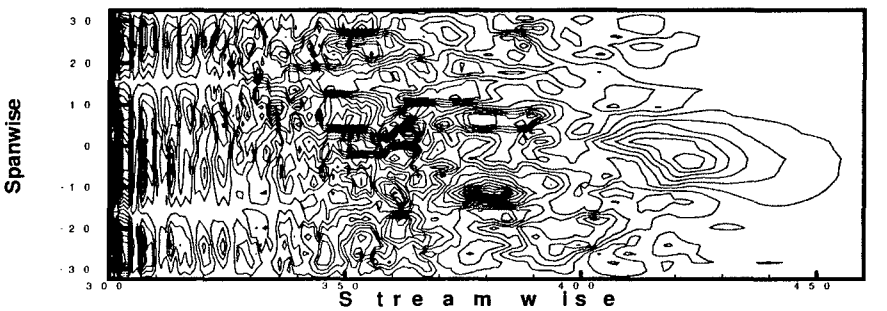


Figure 2, Spanwise velocity contour, Re = 900, F = 86. y = 1.4

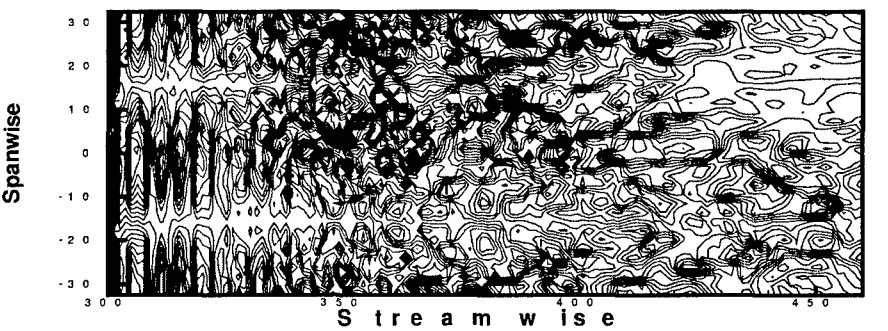


Figure 3, Spanwise velocity contour, Re = 800, F = 86. y = 2.0

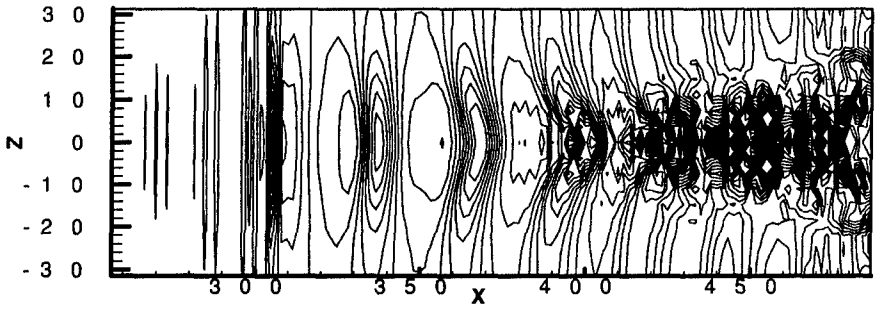


Figure 4, Pressure contour, Re = 900, F = 86. y = 2.0, t = 7T, Ribbon position x = 303.94

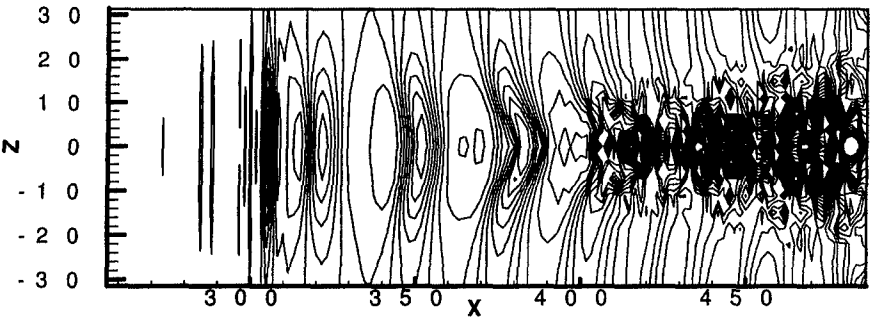


Figure 5, Pressure contour, Re = 900, F = 86. y = 2.0, t = 7.125T, Ribbon position x = 303.94

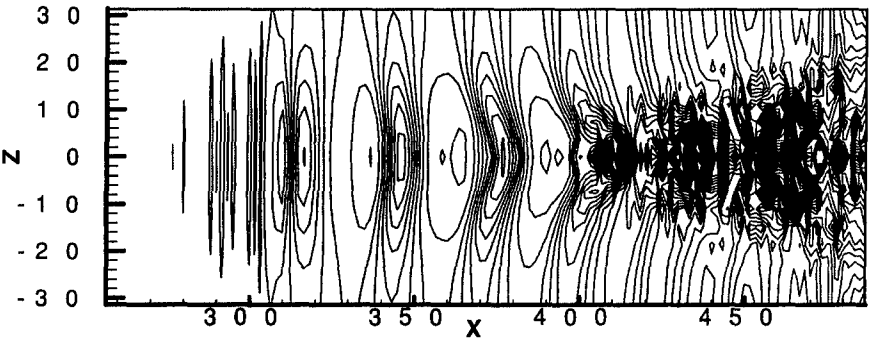


Figure 6, Pressure contour, Re = 900, F = 86. y = 2.0, t = 7. 25T, Ribbon position x = 303.94

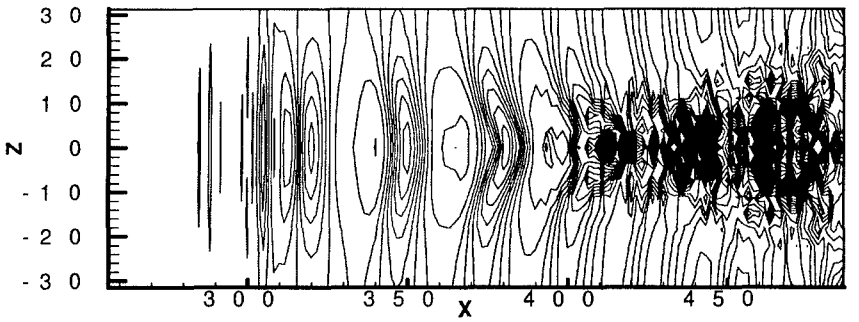


Figure 7, Pressure contour, Re = 900, F = 86. y = 2.0, t = 7. 375T, Ribbon position x = 303.94

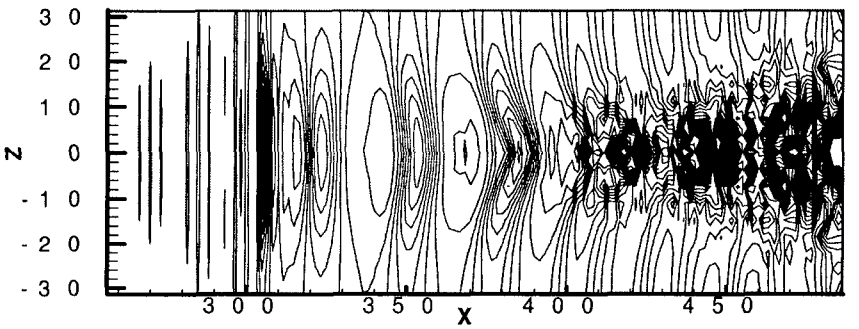


Figure 8, Pressure contour, Re = 900, F = 86. y = 2.0, t = 7. 5T, Ribbon position x = 303.94

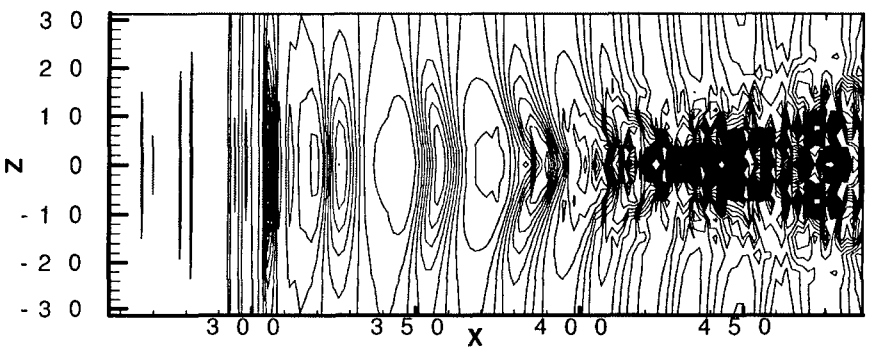


Figure 9, Pressure contour, Re = 900, F = 86. y = 2.0, t = 7. 625T, Ribbon position x = 303.94

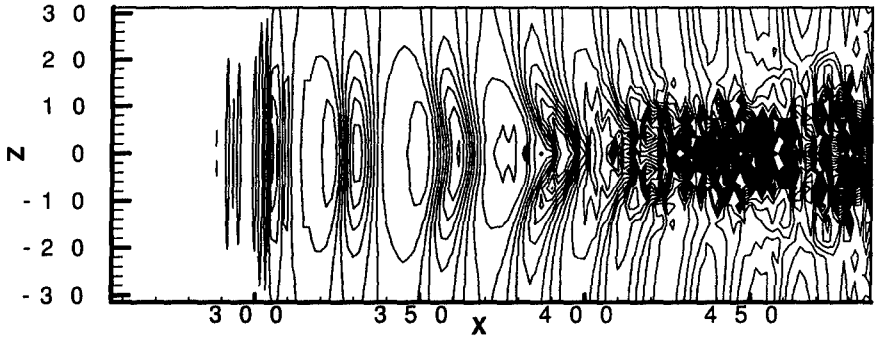


Figure 10, Pressure contour, Re = 900, F = 86. y = 2.0, t = 7. 75T, Ribbon position x = 303.94

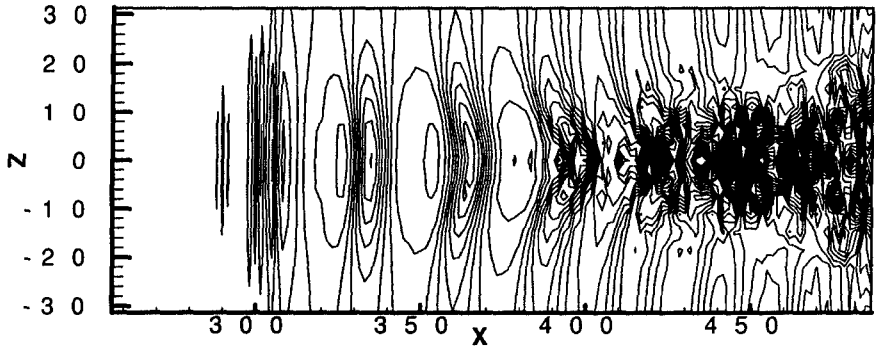


Figure 11, Pressure contour, Re = 900, F = 86. y = 2.0, t = 7. 875T, Ribbon position x = 303.94